THE JOURNAL OF PHYSICAL CHEMISTRY B

Article

Cite This: J. Phys. Chem. B 2018, 122, 10669−10677

pubs.acs.org/JPCB

On the Use of Q-Band Double Electron−Electron Resonance To Resolve the Relative Orientations of Two Double Histidine-Bound Cu^{2+} Ions in a Protein

Austin Gamble Jarvi,[†] Kalina Ranguelova,[‡] Shreya Ghosh,[†] Ralph T. Weber,[‡] and Sunil Saxena*[,†]

[†]Department of Chemistry, University of Pittsburgh, Pittsburgh, Pennsylvania 15260, United States

[‡]Bruker BioSpin, Inc., EPR Division, 15 Fortune Drive, Billerica, Massachusetts 01821, United States

Supporting Information

ABSTRACT: In this work, we explore the potential of a rigid Cu^{2+} spin-labeling technique, the double histidine (dHis) motif, along with Q-band electron paramagnetic resonance to report on the relative orientations of the spin labels. We show that the precision of the dHis motif, coupled with the sensitivity and resolution of Q-band frequencies, may allow for the straightforward determination of the relative orientation of the dHis-Cu^{2+} labels using double electron−electron resonance (DEER). We performed Q-band DEER measurements at different magnetic fields on a protein containing two dHis Cu^{2+} sites. These measurements exhibited orientational selectivity such that each discrete magnetic field yielded a unique DEER signal. We determined the relative orientation of the two metal centers by simulating the orientationally selective DEER data. These relative orientations were validated by visual analysis of the protein crystal structure modified with dHis sites. The simple visual analysis was shown to agree well with the angular values determined via simulation of the experimental data. The combination of the dHis-Cu^{2+} motif along with the advantages of the Q-band can aid in the accurate measurement of protein structural and conformational dynamics.

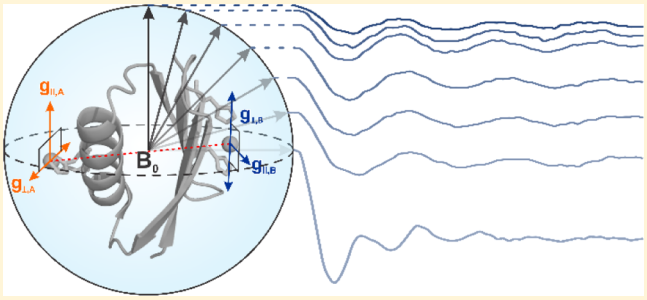

INTRODUCTION

Distance measurements by pulsed electron paramagnetic resonance (EPR) have become important techniques for the determination of macromolecular structure and dynamics.[1,2] These pulsed EPR techniques isolate the weak dipolar coupling between two unpaired electrons in a macromolecule and extract a distance in the range of 2−16 nm.[1−13] Such long-range distance constraints are useful to characterize the structure and flexibility of the macromolecule. Specifically, one exciting application of these EPR distance measurements is the elucidation of induced conformational changes in biomolecules.[1,2,14−20] Such EPR techniques are particularly advantageous for biomolecules that are difficult to crystallize or too large for NMR structural determination.Therefore, pulsed EPR can provide unprecedented insight into the structure and conformations of important biomolecules that would be inaccessible by other means, leading to a greater understanding of the mechanisms of biological processes.

The scope of pulsed EPR methodology has been greatly enhanced by site-directed spin labeling, which typically uses nitroxide-based spin labels.[21−23] Common nitroxide spin labels are versatile[21−26] but can be limited in practice by the long, flexible side chain required to attach the paramagnetic head group to the macromolecular backbone.[27,28] This inherent flexibility translates to broad distance distributions, which can lead to uncertainty in the interpretation of the EPR data in terms of protein structure. Efforts to solve this problem by employing rigid nitroxide labels have met with some success, although these labels are often bulky and far-removed from the protein backbone.[24,29−32]

The demand for alternative spin labels has led to the development of paramagnetic metal-based distance methods and spin-labeling approaches.[33−46] Cu^{2+} specifically has emerged as a simple, site-specific paramagnetic probe that can be incorporated into proteins and DNA to provide precise, accurate distance measurements indicative of the protein or DNA backbone.[42,43,47−49] One such Cu^{2+} labeling technique which has shown great promise is the double histidine (dHis) motif.[43] The dHis motif involves strategic placement of two histidine residues within a protein. For α-helical sites, an i and i + 4 arrangement of two histidine residues allows for simultaneous cis-coordination of Cu^{2+}, whereas in β-sheets, an i and i + 2 arrangement is necessary to place the two histidine residues on the same face of the sheet for metal binding. This motif rigidly binds Cu^{2+} complexed with ligands and can provide distance distributions up to five times

Received: August 8, 2018
Revised: October 22, 2018
Published: October 29, 2018

DOI: 10.1021/acs.jpcb.8b07727
J. Phys. Chem. B 2018, 122, 10669−10677

narrower than common nitroxide spin labels.[43] This drastic increase in precision is invaluable as initial results suggest that the dHis motif produces data dominated by backbone fluctuation rather than side chain mobility. The benefits of the dHis motif were evidenced recently when both nitroxide and dHis-Cu^{2+} distance measurements were applied to the glutathione S-transferase system in order to characterize its conformational equilibrium.[50] The dHis motif provided significantly enhanced resolution over the nitroxide spin labels in this system.[50]

However, even with the added precision that the dHis-Cu^{2+} motif provides, there may be multiple possible conformational states that satisfy a given distance constraint. Therefore, additional structural information may be useful for full elucidation of a given conformation. Orientationally selective double electron−electron resonance (DEER) is one such technique that provides complementary data on the relative orientation of the two spin labels. Orientational selectivity can occur because pulse lengths typically applied in pulsed EPR can only excite a small portion of the total spectrum. In systems containing large *g*-anisotropies and resolved hyperfine anisotropy, excitation of a small portion of the total spectrum can select only a small subset of all possible molecular orientations. At X-band frequencies (9.5 GHz), the nitroxide and Cu^{2+} EPR spectra have large hyperfine splittings relative to the features due to *g*-anisotropy. In this case, the large hyperfine contribution will overlap and mix different features of the spectra, allowing the excitation of multiple orientations within a small spectral region. Orientational selectivity can be further mitigated by using flexible spin labels such that the excited orientations are effectively randomized. This effect is facilitated in nitroxides by their flexible tether to the molecule. In Cu^{2+}-based systems, orientational flexibility of the Cu^{2+} coordination environment achieves the same effect.[51] Therefore, orientational selectivity is uncommon in nitroxide- and Cu^{2+}-based systems at the X-band.

Despite these factors, certain systems exhibit orientational selectivity at the X-band. DEER has been performed on several of these specific nitroxide radical pairs[52−56] and Cu^{2+}−nitroxide systems[57,58] to determine the relative orientations of the spin labels. Such an analysis was also applied to two Cu^{2+} centers within a protein in endogenous binding sites.[59] These methods benefit from higher frequency EPR spectrometers, such as Q-band (35 GHz) and W-band (95 GHz), becoming more accessible. Their increased resolution can enhance orientational selectivity and leads to easier disentanglement of spin-label orientations.[60−67] Recently, Q-band EPR has been used to assess the general orientations of Cu^{2+} centers in DNA G-quadruplexes.[68] Additionally, rigid spin labels have been employed for similar studies.[56,69] Despite all these efforts, the current state of orientational selectivity analysis using rigid Cu^{2+} labels at the Q-band is limited, and it is therefore of interest to refine this method and demonstrate its applicability to a wider variety of biomolecules.

Herein, we show that Q-band orientationally selective DEER using the dHis motif provides a simple, reliable method of determining Cu^{2+} label orientation within a macromolecule. We demonstrate that Q-band DEER is sensitive to the relative orientations of Cu^{2+} within the dHis motif. Additionally, we show that the relative orientations can be determined through simulation of the orientationally selective DEER data. Last, we show that the relative orientations determined via simulation agree with an intuitive visual analysis of the protein crystal structure.

EXPERIMENTAL SECTION

For our experiments, we used a 6H/8H/28H/32H mutant of the immunoglobulin-binding domain of protein G, called GB1. The protein expression and purification of the GB1 tetramutant were performed as described elsewhere.[43,48] Cu^{2+} was complexed with nitrilotriacetic acid (NTA) prior to its introduction to the protein. All EPR samples were prepared in 50 mM *N*-ethylmorpholine buffer at pH 7.4 with 20% glycerol as a cryoprotectant with a ratio of GB1−Cu^{2+}−NTA of 1:1.5:1.5.

DEER data were acquired with a Bruker E680 spectrometer equipped with a 150 W amplifier and an ER5106 QT2 resonator. The sample temperature of 20 K was maintained using a Bruker B8692690 cryogen free cryostat. The resonator was overcoupled to a bandwidth of 250 MHz. The pump microwave frequency was set to the center of the resonator dip to optimize modulation depth, and the observer frequency was set 100 MHz higher in frequency. π pulse lengths of 28 and 50 ns were attained for pump and observer frequencies, respectively. To increase the modulation depth, an 80 ns chirp pulse with the frequency range of −150 to −50 MHz relative to the observer frequency was used. A four pulse DEER with a 16-step phase cycle was performed with the sequence $(\pi/2)_{\omega A}-\tau-(\pi)_{\omega A}-\tau + T-(\pi)_{\omega B}-\tau_2 - T-(\pi)_{\omega A}-\tau_2-$echo.[70] τ was set to 200 ns and data were collected over a time interval of 1.3 μs with a step size of 10 ns, resulting in a 128-point data set. The shot repetition was 61.2 μs. Including the 16-step phase cycle, 409 600 averages were acquired. In order to acquire the orientation selection data, a pulse program was written to acquire DEER spectra from 11 020 to 11 774 G at 17 magnetic field values. To determine the distance distribution, these signals were summed and analyzed using the DeerAnalysis software package.[71]

Simulations of the individual time-domain DEER signal were performed using the methodology developed previously by the group, as detailed elsewhere.[51]

Briefly, the DEER signal can be expressed as[51,72,73]

$$V(t) = 1 - \int\int P(r)\left(\lambda - \lambda \cos\left[\frac{k}{r^3}(1 - 3\cos^2\theta)t\right]\right) \xi(\theta)\, d\theta dr \quad (1)$$

where $P(r)$ is the distance distribution, θ is the angle between the interspin vector and the applied magnetic field, k is a constant containing the product of two spins' *g* values, r is the distance between the two spins, and λ is the modulation depth. $\xi(\theta)$ is the geometrical factor, given by[51,73]

$$\xi(\theta) = \frac{1}{2} \sum_{m_{I_1} m_{I_2}} \langle k_{xa}{}^3 k_{xb}{}^2 \sin\varphi_{1a}(1 - \cos\varphi_{2a})(1 - \cos\varphi_{3b}) + k_{xb}{}^3 k_{xa}{}^2 \sin\varphi_{1b}(1 - \cos\varphi_{2b})(1 - \cos\varphi_{3a})\rangle_{\phi,\delta\omega_1,\delta\omega_2} \quad (2)$$

where m_{I_i} is the nuclear quantum number of spin I, φ_{ia} is the flip angle of the first spin by the ith pulse, φ_{ib} is the flip angle of the second spin by the ith pulse, $\delta\omega_1$ is the inhomogeneous broadening of the observer or pump pulses, k_{xa} is the ratio of the resonance frequency of the spins excited by the observer

DOI: 10.1021/acs.jpcb.8b07727
J. Phys. Chem. B 2018, 122, 10669−10677

pulses to the observer frequency, and k_{xb} is the ratio of the resonance frequency of the spins excited by the pump pulse to the pump frequency.

The geometrical factor depends implicitly on the relative orientations of two principle axis systems of the g-tensors of the two Cu^{2+} spins. The relative orientations are described by the angles χ, γ, and η[51] (cf. Figure 1A). χ is the angle between spin A's $g_{\parallel}$ axis and the interspin vector, r. γ is the angle between the $g_{\parallel}$ axes of spin A and B. η is the angle between the $g_{\perp}$ axes of spin A and B. Each of these angles has an associated standard deviation, σ. To limit the number of variables, a single σ was used for all three angles. All other variables were set in accordance with the above experimental parameters.

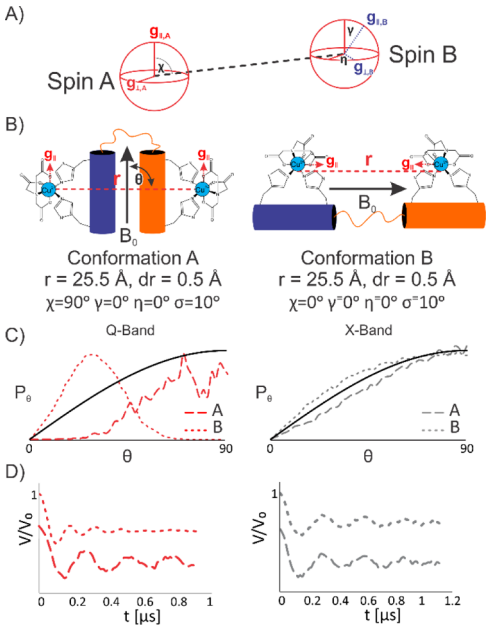

Figure 1. An overview of orientational selectivity and its applications in determining the protein structure and conformation. (A) Brief definition of the angles used to relate two coupled spins in a macromolecule. (B) Two conformations of the same protein, with two dHis mutations. The distances and distributions remain identical, but the orientation of the spin labels is changed. (C) Curves indicate the probability of exciting certain θ in the DEER experiment. This curve and simulations were performed with a sufficient orientational distribution such that orientation effects are washed out at the X-band, consistent with many dHis-based distances observed so far (see text). The curves are indicative of an excitation at $g_{\parallel}$. The black line shows the equal excitation of all orientations. Dashed lines indicate conformation A, and dotted lines indicate conformation B at the Q-band and X-band from left to right. (D) Simulated DEER signals obtained at each frequency for conformations A and B. The dashed line represents A and the dotted represents B.

Simulated DEER signals were normalized and adjusted to match the modulation depth of the experimental signal. Molecular modeling was done using Pymol. Visualization of the Cu^{2+} spin label was achieved using multiscale modeling of macromolecules (MMM).[74,75]

RESULTS AND DISCUSSION

In this work, we examine the potential of Q-band EPR to resolve the relative orientation between two units on a protein. We have shown previously that, in theory, orientational selectivity for Cu^{2+}−Cu^{2+} DEER measurements is a possibility; however, in practice, it is not commonly observed at the X-band.[13,42,76,77] Orientational selectivity can be reduced in Cu^{2+}−DEER because of a distribution in relative orientations of the g-tensor[13,51,76] and in cases due to the specific relative orientations of the g-tensors.[77,78] Similarly, at the X-band, orientational effects on dHis-based distances have not been observed within signal to noise considerations so far.[43,47,48,50]

Q-band orientationally selective DEER can be a powerful probe of spin-label orientation and molecular conformation. The relative orientations of two coupled spins are shown in Figure 1A, along with the angles used to relate the orientations as described previously. Figure 1B shows two conformations of the same macromolecule, with a dHis Cu^{2+}−NTA site on each subunit. We assume that both conformations have the same distance between Cu^{2+} centers, r, and standard deviation, δr. However, the relative orientations of the Cu^{2+} centers are different, where $g_{\parallel}$ is perpendicular to the interspin vector, r, for conformation A and $g_{\parallel}$ is parallel to r for conformation B. At the magnetic field corresponding to $g_{\parallel}$, different θ will be probed, where θ is the angle between r and the applied magnetic field, B_0, as shown in Figure 1B. Excitation probability at this magnetic field for both X and Q-bands is shown in Figure 1C. These probabilities were calculated as the geometrical factor, $\xi(\theta)$[51,73] (cf. eq 2). Difference in θ excited can be shown by the probability curves in Figure 1C. These curves depict the probability distribution of θ, P_{θ}, that is excited by a typical pump pulse used in DEER. The black lines in Figure 1C show the probability curve when all molecular orientations are excited or the ideal case for DEER. The left and right frames show the probability curves at the Q-band and X-band, respectively, for conformations A and B. For the parameters given, χ = 90°, γ = 0°, η = 0°, and σ = 10° for conformation A and χ = 0°, γ = 0°,η = 0°, and σ = 10° for conformation B. With σ = 10°, orientational effects are washed out at the X-band.[51] The $\xi(\theta)$ is different at Q-band versus X-band. At the Q-band, we can see that the θ probed varies greatly between conformations A and B, despite the orientational distribution, whereas at the X-band, orientational selectivity is washed out and the difference between the two excitations is negligible. Figure 1D shows the DEER signals that result from each excitation. Again, the DEER signals produced at the Q-band are distinctly different from each other, whereas the X-band data show identical modulations. Under such conditions of a large orientational flexibility (i.e., σ = 10°) at the X-band, the two conformations cannot be distinguished by DEER. However, using the Q-band, orientational selectivity is easily manifested in DEER, allowing the relative orientations of the spin labels to be determined. Therefore, determination of spin-label orientation may enable new avenues of structural and conformational characterization of proteins and macromolecules. It should be noted that Figure 1 presents the simplest case, with colinear $g_{\parallel}$ axes. The principles shown in Figure 1 are also applicable to systems with orthogonal g-tensors (Figure S1), and both modulation frequency and modulation depth may be indicators of orientational selectivity.

To explore this potential, we chose the B1 immunoglobulin-binding domain of protein G (GB1) modified with two dHis motifs at sites 6H/8H and 28H/32H for our orientational selectivity analysis.[43] GB1 is a simple model system that is thermally stable,[79,80] has been extensively characterized by EPR and other methods[81−89] and has served as the template on which the dHis motif was designed,[43,47,48] making it ideal

DOI: 10.1021/acs.jpcb.8b07727
J. Phys. Chem. B 2018, 122, 10669−10677

for our purposes. The rigidity of the dHis motif provides well-defined, unambiguous dipolar modulations in the DEER experiment[43] that aids in clarifying the orientational effects. Cu^{2+} used in this work is chelated with the NTA ligand, which has been shown to prevent nonspecific binding of Cu^{2+} and increases binding affinity to α-helical sites compared to similar ligands.[48]

The orientation of such Cu^{2+} in the dHis motif is defined by the coordinating ligands. Cu^{2+} most commonly exhibits octahedral coordination geometry, with four equatorial ligands defining its $g_\perp$ plane and two axial ligands defining the $g_\parallel$ axis. For Cu^{2+}–NTA in the dHis motif, the coordination geometry is shown in Figure 2A. The imidazole nitrogens of the histidine

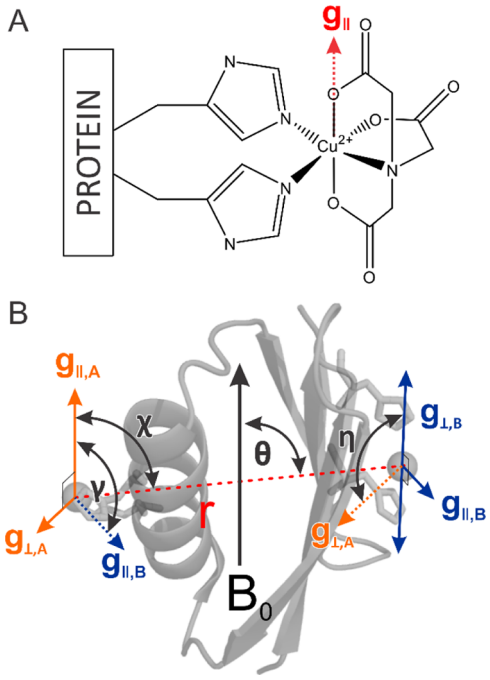

Figure 2. (A) Proposed coordination environment of Cu^{2+} chelated with NTA within the dHis motif. The imidazole nitrogens are expected to bind in two equatorial positions, allowing for simple determination of the Cu^{2+} orientation based on the dHis position. (B) Molecular model used in the DEER simulations. The principal axis systems for the *g*-tensors of spin A (orange) and B (blue) are shown overlaid on the crystal structure of 6H/8H/28H/32H GB1 (PDB: 4WH4). The relative orientations of these principal axis systems are defined relative to each other based on three angles: χ, γ, and η.

residues coordinate to Cu^{2+} in two equatorial positions. Therefore, we can estimate that the $g_\perp$ plane contains Cu^{2+} and the coordinating nitrogens. $g_\parallel$ is along the axially coordinated oxygen atoms from the NTA chelator and points perpendicular to the $g_\perp$ plane. In this way, we can define the orientations of the Cu^{2+} spin labels within the overall molecular frame. By determining the orientation of both spin labels with respect to each other, we can gain insight on the overall structure and conformation of the molecule.

Figure 2B shows a crystal structure of 6H/8H/28H/32H GB1 (PDB: 4WH4).[43] This crystal structure was determined without Cu^{2+}; therefore, Cu^{2+} ions were placed in the structure in silico according to previous methods.[43] Using the definitions above, we have superimposed the proposed $g_\parallel$ and $g_\perp$ axes over each Cu^{2+} ion. To reiterate, we can then define a set of angles to relate the two axis systems: χ, γ, and η.[51] χ is the angle between spin A's $g_\parallel$ axis and the interspin vector, *r*. γ is the angle between the $g_\parallel$ axes of spin A and B. η is the angle between the $g_\perp$ axes of spin A and B. Another angle, θ, is the angle between the applied magnetic field vector and the interspin vector, *r*. θ is not necessary to define the relative orientations of the spin labels but describes the overall molecular orientation. With the molecular model defined, pulsed EPR can then be used to extract the relative orientations of the Cu^{2+} labels.

To this end, we first collected DEER data at multiple magnetic fields between $g_\parallel$ and $g_\perp$ at Q-band frequencies to probe the extent of orientational selectivity in the system. Figure 3A shows the field-swept spectrum and the magnetic fields at which DEER was performed as indicated on the spectrum. A total of 17 DEER signals were collected, ranging from 11 774 to 11 020 G to obtain a sufficiently robust set of data. The corresponding DEER signals are shown in Figure 3B. Interestingly, the modulation frequency decreases as the magnetic field decreases, clearly demonstrating the orientational selectivity effect at the Q-band. The modulation depth of the DEER signal decreases at lower magnetic fields. This effect is due in part to the intensity of the absorption spectrum decreasing along with the magnetic field and also due to orientational selectivity.

We then summed the raw Q-band DEER signals to compare with previously collected X-band data. In previously published work, the system did not exhibit orientational selectivity at the X-band and therefore one DEER signal collected at the $g_\perp$ field position sufficed.[43,48] This supposition was confirmed experimentally, in which DEER was performed on the sample at the X-band at $g_\perp$ and $g_\parallel$ which produced identical distance distributions (Figure S2). Figure 3C shows DEER signals collected at the X-band and the summed Q-band. Clearly, the modulation frequency is similar between the two runs. The resultant distance distributions as analyzed by Tikhonov regularization[90] are shown in Figure 3D. The most probable distances of each distribution are 2.44 nm for the X-band and 2.40 nm for the Q-band, which agree well within the uncertainty of the measurement as shown by the validation in Figure 3D. Furthermore, the distance distributions inform us of the distance and the standard deviation to be used for simulation.

Next, we simulated the data in order to determine the angle parameters using the methodology previously developed by our group.[51] Figure 4 shows the results of these simulations, where the black lines show the experimental DEER signals and the colored lines show the simulated DEER signals for the respective magnetic fields. This methodology simulates a DEER signal based on user provided experimental parameters. These parameters include the three angles, χ, γ, and η, with associated standard deviations, σ_χ, σ_γ, and σ_η, for a given Gaussian distance distribution with distance *r* and standard deviation d*r*. Thus, by specifying the magnetic field used in each DEER trace and holding all other variables constant, we can generate a series of simulated DEER signals to compare with the experimental results.

The *g* and *hf* values have been determined for the dHis Cu^{2+} site previously, where r = 25.5 Å, dr = 0.5 Å, $g_\perp$ = 2.064, $g_\parallel$ = 2.277, $A_\perp$ = 25 G, and $A_\parallel$ = 175 G.[48] Thus, we focused on fitting the three main angles χ, γ, and η and σ_χ, σ_γ, and σ_η. In order to reduce the number of variables, we set $\sigma_\chi = \sigma_\gamma = \sigma_\eta \equiv \sigma$. From the analysis of $g_\parallel$ and $g_\perp$ field positions above, we set χ to 90° initially and varied γ and η systematically from 0° to 90°

DOI: 10.1021/acs.jpcb.8b07727
J. Phys. Chem. B 2018, 122, 10669–10677

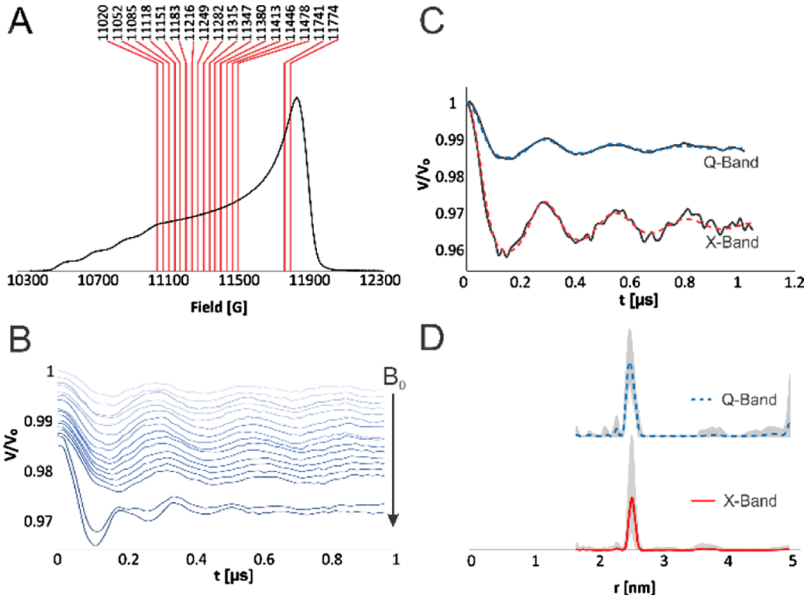

Figure 3. (A) Field-swept Cu^{2+} spectrum. The red lines indicate field positions at which DEER was performed. (B) Experimental DEER data as a function of magnetic field to demonstrate the effects of orientational selectivity. (C) Summation of the Q-band DEER signals as compared with X-band DEER, which serves as a validation of the Q-band data. (D) Distance distributions via Tikhonov regularization of the summed Q-band data compared to the X-band data. The gray shading indicates the uncertainty in the distance analysis.

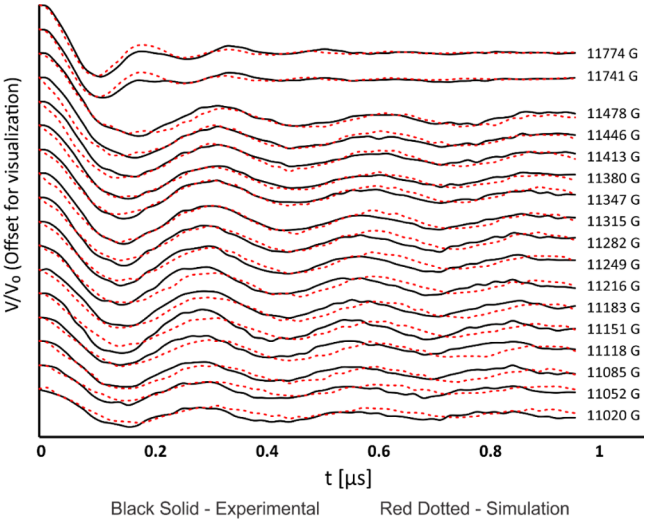

Figure 4. Experimental DEER signals (black) and their corresponding simulations (red dashed) offset on the *y*-axis for ease of visualization. The simulated DEER signals used the best set of angle parameters with r = 25.5 Å, δr = 0.5 Å, χ = 80°, γ = 75°, and η = 22.5° and $\sigma_\chi = \sigma_\gamma = \sigma_\eta$ = 10°.

at 10° intervals until a reasonable fit was reached. Each angle was then varied about this reasonable set by smaller intervals until the best fit was reached. This was found to be at χ = 80°, γ = 75°, and η = 22.5° and $\sigma_\chi = \sigma_\gamma = \sigma_\eta$ = 10°. Figure 4 shows that the simulations provide a good fit to the experimental data across the range of magnetic fields sampled.

Because the orientational term of the DEER signal is dependent on $\cos^2(\theta)$ (eq 1), one must consider the issue of symmetric solutions.[67] To understand this issue, we performed additional simulations using the best fit parameters ascertained above and incrementing each angle by 90° (Figures S3 and S4). Based on these simulations, we found that the angles χ and γ exhibited a 180° symmetry such that for either angle α, α and α + 180° produced identical dipolar traces. To confirm this point, we performed an identical analysis using a different set of angles to remove any bias toward our results: χ = 30°, γ = 60°, and η = 90° (Figures S5 and S6). This new set of parameters matched the previous results in which we observed a 180° symmetry for χ and γ. Because χ and γ are doubly degenerate, there are 2^2 possible sets of angles that will adequately satisfy the simulations (Figure S7). Because of the axial symmetry of Cu^{2+}, the direction of the $g_\parallel$ axis cannot be absolutely defined, and therefore, there is some ambiguity in this set of solutions.[59]

Importantly, the angular results determined from simulations are in agreement with a basic visual analysis of the 6H/8H/28H/32H-modified GB1 crystal structure (PDB: 4WH4).[43] This tetramutant was crystallized in the absence of Cu^{2+}. We placed Cu^{2+} ions in the structure in silico and positioned them with respect to the histidines based on the structure of a Cu^{2+} ion coordinated to two imidazole ligands[91] as was done previously.[43] Figure 5 shows this structure. To perform a visual analysis, we superimposed the proposed *g*-tensor axes on the crystal structure. Based on previous work, it is assumed that the imidazole nitrogens coordinate to Cu^{2+} in the dHis motif along two of the equatorial sites.[43,48] Therefore, from the crystal structure, we can estimate that the $g_\perp$ plane is formed by the Cu^{2+} ion and the two coordinating nitrogens. As well, the $g_\parallel$ axis can be estimated as perpendicular to the $g_\perp$ plane. From these axes, the angles are easily calculated, as shown. Figure 5 shows these axes from various perspectives such that all three angles χ, γ, and η can be easily visualized and determined. Based on the above model shown in Figure 5, we can measure the angles χ, γ, and η directly from the given crystal structure. From the crystal structure, $\chi \approx 77-84°$, $\gamma \approx 74°$, and $\eta \approx 19°$. These values agree well with the best-fit simulation parameters: χ = 80°, γ = 75°, and η = 22.5°.

Furthermore, the crystal structure analysis supports the Q-band DEER data. Figure 6A shows a molecular orientation found at $g_\parallel$, based on our visual analysis. Figure 6B shows the

DOI: 10.1021/acs.jpcb.8b07727
J. Phys. Chem. B 2018, 122, 10669−10677

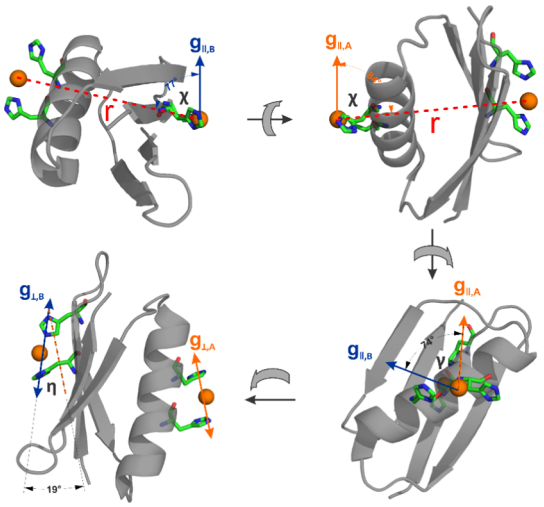

Figure 5. Visualization and basic analysis of the expected χ, γ, and η values determined from the crystal structure. Each pane shows an estimate of the direction of an element of the Cu^{2+} g-tensor overlaid on the dHis-modified GB1 crystal structure (PDB: 4WH4). The three angles can then be determined from simple graphical analysis. The angles determined in this way agree well with those determined by simulation.

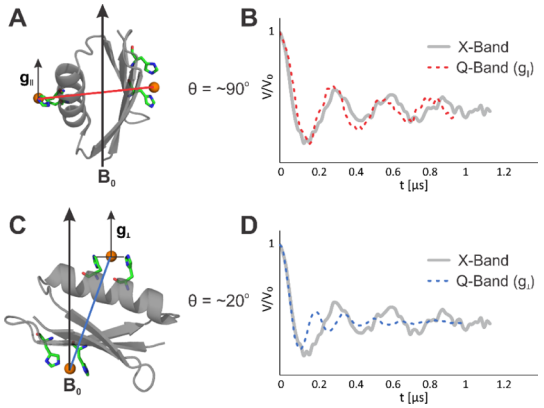

Figure 6. (A,C) Molecular orientations of GB1 corresponding to the $g_{\parallel}$ and $g_{\perp}$ regions, respectively. (B,D) Resulting DEER signals dictated by the θ orientations selected by the orientations in (A,C), respectively.

Q-band DEER signal collected near $g_{\parallel}$ (red dashed) compared to the orientationally averaged X-band signal (gray). From the θ probability curves shown in Figure 1C, it is clear that the orientation-averaged ω_{Dip} is dominated by the θ = 90° orientation. The agreement between the Q-band and X-band modulation frequencies in Figure 6B indicates that the orientations selected at $g_{\parallel}$ are likewise dominated by θ = 90°. In Figure 6A, the interspin vector is approximately perpendicular to B_0, such that this condition is true. Likewise, Figure 6C,D shows corresponding data at $g_{\perp}$. From Figure 6C, the θ at $g_{\perp}$ selected is not close to 90°. Accordingly, Figure 6D shows that the modulation frequency at $g_{\perp}$ (blue dashed) does not agree with the X-band data (gray). This analysis further illustrates the sensitivity of Q-band DEER to the relative orientations of the Cu^{2+} labels.

We further applied our simple visual analysis to the standard deviations of χ, γ, and η. MMM is a type of software that labels a given protein with the dHis Cu^{2+}–NTA motif and calculates a spatial distribution of the Cu^{2+} location.[74,75] The positions of the Cu^{2+} centers can then be visualized. Figure 7 shows the

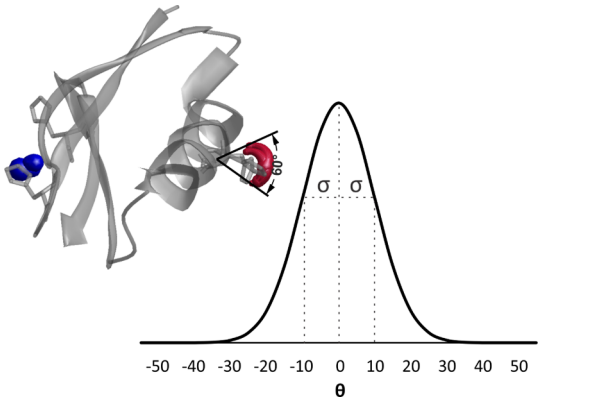

Figure 7. Visual analysis of the standard deviations of the angles derived from simulation. Inset shows the GB1 crystal structure with Cu^{2+} positions shown in red and blue. The angular range of Cu^{2+} positions was estimated graphically as a total of 60°. A Gaussian distribution with a standard deviation of 10° is shown, where the total range is also approximately 60°.

dHis-modified GB1 crystal structure labeled with the Cu^{2+}–NTA complex via MMM. The locations of the Cu^{2+} centers are shown in red and blue. The 6H/8H Cu^{2+} (blue) position is largely globular which leads to an ambiguous visual analysis; however, 28H/32H Cu^{2+} (red) provides some insight into appropriate σ. The histidine residues are shown in Figure 7. We note that the 28H/32H Cu^{2+} positions fluctuate primarily in an arc that rotates about C_{α} of the His residues. The arc in question was measured to span 60°. This angle can be easily related to η, as it is directly linked to flexibility in the $g_{\perp}$ plane formed by Cu^{2+} and the His nitrogens. However, because $g_{\parallel}$ is perpendicular to this plane, it will also experience a 60° variance. Therefore, this range is extended to χ as well. If we assume a Gaussian distribution about the mean position, a σ of 10° produces distribution with a total range of 60°. This distribution is shown in Figure 7. Additionally, a σ of 10° agrees with previous findings regarding the Cu^{2+} g-tensor, in which a 10° standard deviation washed out orientational selectivity at the X-band,[51] which is consistent for this system.

CONCLUSIONS

In conclusion, we have shown the potential of Q-band orientationally selective DEER in conjunction with the rigid Cu^{2+}-binding dHis motif to provide constraints on the relative orientations of the Cu^{2+} g-tensors. We have simulated a full set of orientationally selective Q-band DEER to extract the relative orientations of the Cu^{2+} g-tensors. These results agreed well with the relative orientations determined from a simple visual analysis of the protein crystal structure. The agreement demonstrates that Q-band orientationally selective DEER can be used to determine physically meaningful spin-label orientations. Likewise, the orientations of the Cu^{2+} centers in the dHis motif can be determined directly from the crystal structure. Therefore, Q-band DEER using the dHis Cu^{2+} motif can easily provide additional insight into the protein structure and conformational determination.

DOI: 10.1021/acs.jpcb.8b07727
J. Phys. Chem. B 2018, 122, 10669–10677

■ ASSOCIATED CONTENT

Supporting Information

The Supporting Information is available free of charge on the ACS Publications website at DOI: 10.1021/acs.jpcb.8b07727.

Overview of orientational selectivity on a system with orthogonal g-tensors, DEER data on 6H/8H/28H/32H GB1, simulated DEER signals at magnetic fields 11774 G and 11020 G at Q-band frequency, simulated DEER signals at magnetic fields 11183 G and 11347 G, simulated DEER signals at magnetic fields 11774 G and 11020 G, simulated DEER signals at magnetic fields 11183 G and 11347 G, and alternative angular parameters for the best-fit relative orientations (PDF)

■ AUTHOR INFORMATION

Corresponding Author

*E-mail: sksaxena@pitt.edu. Phone: 412 624 8680.

ORCID

Sunil Saxena: 0000-0001-9098-6114

Notes

The authors declare no competing financial interest.

■ ACKNOWLEDGMENTS

These data were supported by the National Science Foundation (NSF MCB-1613007). The EPR spectrometer was supported by the National Science Foundation (NSF MRI-1725678). We thank Prof. Zhongyu Yang (North Dakota State University) for his advice and guidance regarding the simulations.

■ REFERENCES

(1) Borbat, P. P.; Freed, J. H. Pulse dipolar ESR: Distance measurements. In *Structural Information from Spin-Labels and Intrinsic Paramagnetic Centers in the Biosciences*; Timmel, C. R., Harmer, J. R., Eds.; Structure and Bonding; Springer: New York, USA, 2012; pp 1−82.

(2) Jeschke, G. DEER distance measurements on proteins. *Annu. Rev. Phys. Chem.* **2012**, *63*, 419−446.

(3) Milov, A. D.; Maryasov, A. G.; Tsvetkov, Y. D. Pulsed electron double resonance (PELDOR) and its applications in free-radicals research. *Appl. Magn. Reson.* **1998**, *15*, 107−143.

(4) Pannier, M.; Veit, S.; Godt, A.; Jeschke, G.; Spiess, H. W. Dead-time free measurement of dipole-dipole interactions between electron spins. *J. Magn. Reson.* **2000**, *142*, 331−340.

(5) Saxena, S.; Freed, J. H. Double quantum two-dimensional Fourier transform electron spin resonance: Distance measurements. *Chem. Phys. Lett.* **1996**, *251*, 102−110.

(6) Kulik, L. V.; Dzuba, S. A.; Grigoryev, I. A.; Tsvetkov, Y. D. Electron dipole−dipole interaction in ESEEM of nitroxide biradicals. *Chem. Phys. Lett.* **2001**, *343*, 315−324.

(7) Milikisyants, S.; Scarpelli, F.; Finiguerra, M. G.; Ubbink, M.; Huber, M. A pulsed EPR method to determine distances between paramagnetic centers with strong spectral anisotropy and radicals: the dead-time free RIDME sequence. *J. Magn. Reson.* **2009**, *201*, 48−56.

(8) Jeschke, G.; Pannier, M.; Godt, A.; Spiess, H. W. Dipolar spectroscopy and spin alignment in electron paramagnetic resonance. *Chem. Phys. Lett.* **2000**, *331*, 243−252.

(9) Schmidt, T.; Wälti, M. A.; Baber, J. L.; Hustedt, E. J.; Clore, G. M. Long distance measurements up to 160 Å in the GroEL tetradecamer using Q-Band DEER EPR spectroscopy. *Angew. Chem.* **2016**, *128*, 16137−16141.

(10) Becker, J. S.; Saxena, S. Double quantum coherence electron spin resonance on coupled Cu(II)-Cu(II) electron spins. *Chem. Phys. Lett.* **2005**, *414*, 248−252.

(11) Ruthstein, S.; Ji, M.; Mehta, P.; Jen-Jacobson, L.; Saxena, S. Sensitive Cu2+-Cu2+ distance measurements in a protein-DNA complex by DQC ESR. *J. Phys. Chem. B* **2013**, *117*, 6227−6230.

(12) Ruthstein, S.; Ji, M.; Shin, B.-k.; Saxena, S. A simple double quantum coherence ESR sequence that minimizes nuclear modulations in Cu 2+-ion based distance measurements. *J. Magn. Reson.* **2015**, *257*, 45−50.

(13) Ji, M.; Ruthstein, S.; Saxena, S. Paramagnetic metal ions in pulsed ESR distance distribution measurements. *Acc. Chem. Res.* **2013**, *47*, 688−695.

(14) Schiemann, O.; Prisner, T. F. Long-range distance determinations in biomacromolecules by EPR spectroscopy. *Q. Rev. Biophys.* **2007**, *40*, 1−53.

(15) Berliner, L. J.; Eaton, S. S.; Eaton, G. R. *Distance Measurements in Biological Systems by EPR*; Springer Science & Business Media, 2006; Vol. *19*.

(16) Reginsson, G. W.; Schiemann, O. Pulsed electron-electron double resonance: beyond nanometre distance measurements on biomacromolecules. *Biochem. J.* **2011**, *434*, 353−363.

(17) Chakrapani, S. EPR studies of gating mechanisms in ion channels. *Methods Enzymol.* **2015**, *557*, 279−306.

(18) Cafiso, D. S. Identifying and quantitating conformational exchange in membrane proteins using site-directed spin labeling. *Acc. Chem. Res.* **2014**, *47*, 3102−3109.

(19) Glaenzer, J.; Peter, M. F.; Hagelueken, G. Studying structure and function of membrane proteins with PELDOR/DEER spectroscopy − A crystallographers' perspective. *Methods* **2018**, *147*, 163−175.

(20) Stone, K. M.; Townsend, J. E.; Sarver, J.; Sapienza, P. J.; Saxena, S.; Jen-Jacobson, L. Electron spin resonance shows common structural features for different classes of Ecori−DNA complexes. *Angew. Chem.* **2008**, *120*, 10346−10348.

(21) Hubbell, W. L.; Mchaourab, H. S.; Altenbach, C.; Lietzow, M. A. Watching proteins move using site-directed spin labeling. *Structure* **1996**, *4*, 779−783.

(22) Jeschke, G.; Polyhach, Y. Distance measurements on spin-labelled biomacromolecules by pulsed electron paramagnetic resonance. *Phys. Chem. Chem. Phys.* **2007**, *9*, 1895−1910.

(23) Hubbell, W. L.; López, C. J.; Altenbach, C.; Yang, Z. Technological advances in site-directed spin labeling of proteins. *Curr. Opin. Struct. Biol.* **2013**, *23*, 725−733.

(24) Haugland, M. M.; Lovett, J. E.; Anderson, E. A. Advances in the synthesis of nitroxide radicals for use in biomolecule spin labelling. *Chem. Soc. Rev.* **2018**, *47*, 668−680.

(25) Roser, P.; Schmidt, M. J.; Drescher, M.; Summerer, D. Site-directed spin labeling of proteins for distance measurements in vitro and in cells. *Org. Biomol. Chem.* **2016**, *14*, 5468−5476.

(26) Shelke, S. A.; Sigurdsson, S. T. Site-directed spin labeling for EPR studies of nucleic acids. In *Modified Nucleic Acids*; Nakatani, K., Tor, Y., Eds.; Springer International Publishing: Cham, 2016; pp 159−187.

(27) Jeschke, G. Conformational dynamics and distribution of nitroxide spin labels. *Prog. Nucl. Magn. Reson. Spectrosc.* **2013**, *72*, 42−60.

(28) Polyhach, Y.; Bordignon, E.; Jeschke, G. Rotamer libraries of spin labeled cysteines for protein studies. *Phys. Chem. Chem. Phys.* **2011**, *13*, 2356−2366.

(29) Columbus, L.; Kálai, T.; Jekö, J.; Hideg, K.; Hubbell, W. L. Molecular motion of spin labeled side chains in alpha-helices: Analysis by variation of side chain structure. *Biochemistry* **2001**, *40*, 3828−3846.

(30) Fawzi, N. L.; Fleissner, M. R.; Anthis, N. J.; Kálai, T.; Hideg, K.; Hubbell, W. L.; Clore, G. M. A rigid disulfide-linked nitroxide side chain simplifies the quantitative analysis of PRE data. *J. Biomol. NMR* **2011**, *51*, 105−114.

(31) Fleissner, M. R.; Bridges, M. D.; Brooks, E. K.; Cascio, D.; Kalai, T.; Hideg, K.; Hubbell, W. L. Structure and dynamics of a conformationally constrained nitroxide side chain and applications in

EPR spectroscopy. *Proc. Natl. Acad. Sci. U.S.A.* **2011**, *108*, 16241−16246.
(32) Warshaviak, D. T.; Khramtsov, V. V.; Cascio, D.; Altenbach, C.; Hubbell, W. L. Structure and dynamics of an imidazoline nitroxide side chain with strongly hindered internal motion in proteins. *J. Magn. Reson.* **2013**, *232*, 53−61.
(33) Keller, K.; Zalibera, M.; Qi, M.; Koch, V.; Wegner, J.; Hintz, H.; Godt, A.; Jeschke, G.; Savitsky, A.; Yulikov, M. EPR characterization of Mn(II) complexes for distance determination with pulsed dipolar spectroscopy. *Phys. Chem. Chem. Phys.* **2016**, *18*, 25120−25135.
(34) Akhmetzyanov, D.; Plackmeyer, J.; Endeward, B.; Denysenkov, V.; Prisner, T. F. Pulsed electron−electron double resonance spectroscopy between a high-spin Mn2+ ion and a nitroxide spin label. *Phys. Chem. Chem. Phys.* **2015**, *17*, 6760−6766.
(35) Yulikov, M.; Lueders, P.; Warsi, M. F.; Chechik, V.; Jeschke, G. Distance measurements in Au nanoparticles functionalized with nitroxide radicals and Gd3+−DTPA chelate complexes. *Phys. Chem. Chem. Phys.* **2012**, *14*, 10732−10746.
(36) Mascali, F. C.; Ching, H. Y. V.; Rasia, R. M.; Un, S.; Tabares, L. C. Using genetically encodable self-assembling GdIII spin labels to make in-cell nanometric distance measurements. *Angew. Chem.* **2016**, *128*, 11207−11209.
(37) Doll, A.; Qi, M.; Wili, N.; Pribitzer, S.; Godt, A.; Jeschke, G. Gd(III)−Gd(III) distance measurements with chirp pump pulses. *J. Magn. Reson.* **2015**, *259*, 153−162.
(38) Barthelmes, D.; Gränz, M.; Barthelmes, K.; Allen, K. N.; Imperiali, B.; Prisner, T.; Schwalbe, H. Encoded loop-lanthanide-binding tags for long-range distance measurements in proteins by NMR and EPR spectroscopy. *J. Biomol. NMR* **2015**, *63*, 275−282.
(39) Goldfarb, D. Gd3+ spin labeling for distance measurements by pulse EPR spectroscopy. *Phys. Chem. Chem. Phys.* **2014**, *16*, 9685−9699.
(40) Banerjee, D.; Yagi, H.; Huber, T.; Otting, G.; Goldfarb, D. Nanometer-range distance measurement in a protein using Mn2+ tags. *J. Phys. Chem. Lett.* **2012**, *3*, 157−160.
(41) Yang, Z.; Ji, M.; Cunningham, T. F.; Saxena, S. Cu2+ as an ESR Probe of Protein Structure and Function. *Methods Enzymol.* **2015**, *563*, 459−481.
(42) Cunningham, T. F.; Shannon, M. D.; Putterman, M. R.; Arachchige, R. J.; Sengupta, I.; Gao, M.; Jaroniec, C. P.; Saxena, S. Cysteine-specific Cu2+ chelating tags used as paramagnetic probes in double electron electron resonance. *J. Phys. Chem. B* **2015**, *119*, 2839−2843.
(43) Cunningham, T. F.; Putterman, M. R.; Desai, A.; Horne, W. S.; Saxena, S. The Double Histidine Cu2+-Binding Motif: A Highly Rigid, Site-Specific Spin Probe for Electron Spin Resonance Distance Measurements. *Angew. Chem., Int. Ed.* **2015**, *54*, 6330−6334.
(44) Raitsimring, A. M.; Gunanathan, C.; Potapov, A.; Efremenko, I.; Martin, J. M. L.; Milstein, D.; Goldfarb, D. Gd3+ complexes as potential spin labels for high field pulsed EPR distance measurements. *J. Am. Chem. Soc.* **2007**, *129*, 14138−14139.
(45) Abdelkader, E. H.; Lee, M. D.; Feintuch, A.; Cohen, M. R.; Swarbrick, J. D.; Otting, G.; Graham, B.; Goldfarb, D. A new Gd3+ spin label for Gd3+−Gd3+ distance measurements in proteins produces narrow distance distributions. *J. Phys. Chem. Lett.* **2015**, *6*, 5016−5021.
(46) Martorana, A.; Yang, Y.; Zhao, Y.; Li, Q.-F.; Su, X.-C.; Goldfarb, D. Mn(II) tags for DEER distance measurements in proteins via c-s attachment. *Dalton Trans.* **2015**, *44*, 20812−20816.
(47) Lawless, M. J.; Ghosh, S.; Cunningham, T. F.; Shimshi, A.; Saxena, S. On the use of the Cu (II)-iminodiacetic acid complex for double histidine based distance measurements by pulsed ESR. *Phys. Chem. Chem. Phys.* **2017**, *19*, 20959−20967.
(48) Ghosh, S.; Lawless, M. J.; Rule, G. S.; Saxena, S. The Cu2+-nitrilotriacetic acid complex improves loading of α-helical double histidine site for precise distance measurements by pulsed ESR. *J. Magn. Reson.* **2018**, *286*, 163−171.
(49) Lawless, M. J.; Sarver, J. L.; Saxena, S. Nucleotide-independent copper (II)-based distance measurements in DNA by pulsed ESR spectroscopy. *Angew. Chem., Int. Ed.* **2017**, *56*, 2115−2117.
(50) Lawless, M. J.; Pettersson, J. R.; Rule, G. S.; Lanni, F.; Saxena, S. ESR resolves the c terminus structure of the ligand-free human glutathione s-transferase A1-1. *Biophys. J.* **2018**, *114*, 592−601.
(51) Yang, Z.; Kise, D.; Saxena, S. An approach towards the measurement of nanometer range distance based on Cu^{2+} ions and ESR. *J. Phys. Chem. B* **2010**, *114*, 6165−6174.
(52) Lovett, J. E.; Bowen, A. M.; Timmel, C. R.; Jones, M. W.; Dilworth, J. R.; Caprotti, D.; Bell, S. G.; Wong, L. L.; Harmer, J. Structural information from orientationally selective DEER spectroscopy. *Phys. Chem. Chem. Phys.* **2009**, *11*, 6840−6848.
(53) Abé, C.; Klose, D.; Dietrich, F.; Ziegler, W. H.; Polyhach, Y.; Jeschke, G.; Steinhoff, H.-J. Orientation selective DEER measurements on vinculin tail at X-band frequencies reveal spin label orientations. *J. Magn. Reson.* **2012**, *216*, 53−61.
(54) Marko, A.; Prisner, T. F. An algorithm to analyze PELDOR data of rigid spin label pairs. *Phys. Chem. Chem. Phys.* **2013**, *15*, 619−627.
(55) Marko, A.; Margraf, D.; Cekan, P.; Sigurdsson, S. T.; Schiemann, O.; Prisner, T. F. Analytical method to determine the orientation of rigid spin labels in DNA. *Phys. Rev. E: Stat., Nonlinear, Soft Matter Phys.* **2010**, *81*, 021911.
(56) Schiemann, O.; Cekan, P.; Margraf, D.; Prisner, T. F.; Sigurdsson, S. T. Relative orientation of rigid nitroxides by PELDOR: beyond distance measurements in nucleic acids. *Angew. Chem., Int. Ed.* **2009**, *48*, 3292−3295.
(57) Bode, B. E.; Plackmeyer, J.; Prisner, T. F.; Schiemann, O. PELDOR measurements on a nitroxide-labeled Cu(II) porhyrin: orientation selection, spin density distribution, and conformational flexibility. *J. Phys. Chem. A* **2008**, *112*, 5064−5073.
(58) Bode, B. E.; Plackmeyer, J.; Bolte, M.; Prisner, T. F.; Schiemann, O. PELDOR on an exchange coupled nitroxide copper(II) spin pair. *J. Organomet. Chem.* **2009**, *694*, 1172−1179.
(59) Bowen, A. M.; Jones, M. W.; Lovett, J. E.; Gaule, T. G.; McPherson, M. J.; Dilworth, J. R.; Timmel, C. R.; Harmer, J. R. Exploiting orientation-selective DEER: determining molecular structure in systems containing Cu(II) centres. *Phys. Chem. Chem. Phys.* **2016**, *18*, 5981−5994.
(60) Mabbs, F. E.; Collison, D. *Electron Paramagnetic Resonance of d Transition Metal Compounds*; Elsevier, 2013; Vol. *16*.
(61) Denysenkov, V. P.; Prisner, T. F.; Stubbe, J.; Bennati, M. High-frequency 180 GHz PELDOR. *Appl. Magn. Reson.* **2005**, *29*, 375−384.
(62) Denysenkov, V. P.; Biglino, D.; Lubitz, W.; Prisner, T. F.; Bennati, M. Structure of the tyrosyl biradical in mouse R2 ribonucleotide reductase from high-field PELDOR. *Angew. Chem., Int. Ed.* **2008**, *47*, 1224−1227.
(63) Denysenkov, V. P.; Prisner, T. F.; Stubbe, J.; Bennati, M. High-field pulsed electron−electron double resonance spectroscopy to determine the orientation of the tyrosyl radicals in ribonucleotide reductase. *Proc. Natl. Acad. Sci. U.S.A.* **2006**, *103*, 13386−13390.
(64) Sicoli, G.; Argirević, T.; Stubbe, J.; Tkach, I.; Bennati, M. Effects in 94 GHz orientation-selected PELDOR on a rigid pair of radicals with non-collinear axes. *Appl. Magn. Reson.* **2009**, *37*, 539−548.
(65) Kaminker, I.; Tkach, I.; Manukovsky, N.; Huber, T.; Yagi, H.; Otting, G.; Bennati, M.; Goldfarb, D. W-band orientation selective DEER measurements on a Gd3+/nitroxide mixed-labeled protein dimer with a dual mode cavity. *J. Magn. Reson.* **2013**, *227*, 66−71.
(66) Giannoulis, A.; Motion, C. L.; Oranges, M.; Bühl, M.; Smith, G. M.; Bode, B. E. Orientation selection in high-field RIDME and PELDOR experiments involving low-spin CoII ions. *Phys. Chem. Chem. Phys.* **2018**, *20*, 2151−2154.
(67) Tkach, I.; Pornsuwan, S.; Höbartner, C.; Wachowius, F.; Sigurdsson, S. T.; Baranova, T. Y.; Diederichsen, U.; Sicoli, G.; Bennati, M. Orientation selection in distance measurements between nitroxide spin labels at 94 GHz EPR with variable dual frequency irradiation. *Phys. Chem. Chem. Phys.* **2013**, *15*, 3433−3437.

DOI: 10.1021/acs.jpcb.8b07727
J. Phys. Chem. B 2018, 122, 10669−10677

(68) Engelhard, D. M.; Meyer, A.; Berndhäuser, A.; Schiemann, O.; Clever, G. H. Di-Copper (II) DNA G-Quadruplexes as EPR Distance Rulers. *Chem. Commun.* **2018**, *54*, 7455−7458.
(69) Stevens, M. A.; McKay, J. E.; Robinson, J. L. S.; El Mkami, H.; Smith, G. M.; Norman, D. G. The use of the Rx spin label in orientation measurement on proteins, by EPR. *Phys. Chem. Chem. Phys.* **2016**, *18*, 5799−5806.
(70) Tait, C. E.; Stoll, S. Coherent pump pulses in double electron electron resonance spectroscopy. *Phys. Chem. Chem. Phys.* **2016**, *18*, 18470−18485.
(71) Jeschke, G.; Chechik, V.; Ionita, P.; Godt, A.; Zimmermann, H.; Banham, J.; Timmel, C. R.; Hilger, D.; Jung, H. DeerAnalysis 2006 - a comprehensive software package for analyzing pulsed ELDOR data. *Appl. Magn. Reson.* **2006**, *30*, 473−498.
(72) Larsen, R. G.; Singel, D. J. Double electron-electron resonance spin-echo modulation: Spectroscopic measurement of electron spin pair separations in orientationally disordered solids. *J. Chem. Phys.* **1993**, *98*, 5134−5146.
(73) Maryasov, A. G.; Tsvetkov, Y. D.; Raap, J. Weakly coupled radical pairs in solids: ELDOR in ESE structure studies. *Appl. Magn. Reson.* **1998**, *14*, 101−113.
(74) Jeschke, G. MMM: A toolbox for integrative structure modeling. *Protein Sci.* **2018**, *27*, 76−85.
(75) Ghosh, S.; Saxena, S.; Jeschke, G. Rotamer modelling of Cu(II) spin labels based on the double-histidine motif. *Appl. Magn. Reson.* **2018**, *49*, 1281.
(76) Yang, Z.; Kurpiewski, M. R.; Ji, M.; Townsend, J. E.; Mehta, P.; Jen-Jacobson, L.; Saxena, S. ESR spectroscopy identifies inhibitory Cu^{2+} sites in a DNA-modifying enzyme to reveal determinants of catalytic specificity. *Proc. Natl. Acad. Sci. U.S.A.* **2012**, *109*, E993−E1000.
(77) Yang, Z.; Becker, J.; Saxena, S. On Cu(II)-Cu(II) distance measurements using pulsed electron electron double resonance. *J. Magn. Reson.* **2007**, *188*, 337−343.
(78) Merz, G. E.; Borbat, P. P.; Pratt, A. J.; Getzoff, E. D.; Freed, J. H.; Crane, B. R. Copper-Based Pulsed Dipolar ESR Spectroscopy as a Probe of Protein Conformation Linked to Disease States. *Biophys. J.* **2014**, *107*, 1669−1674.
(79) Gronenborn, A.; Filpula, D.; Essig, N.; Achari, A.; Whitlow, M.; Wingfield, P.; Clore, G. A novel, highly stable fold of the immunoglobulin binding domain of streptococcal protein G. *Science* **1991**, *253*, 657−661.
(80) Alexander, P.; Fahnestock, S.; Lee, T.; Orban, J.; Bryan, P. Thermodynamic analysis of the folding of the streptococcal protein G IgG-binding domains B1 and B2: why small proteins tend to have high denaturation temperatures. *Biochemistry* **1992**, *31*, 3597−3603.
(81) Dockter, C.; Volkov, A.; Bauer, C.; Polyhach, Y.; Joly-Lopez, Z.; Jeschke, G.; Paulsen, H. Refolding of the integral membrane protein light-harvesting complex II monitored by pulse EPR. *Proc. Natl. Acad. Sci. U.S.A.* **2009**, *106*, 18485−18490.
(82) Walsh, J. D.; Meier, K.; Ishima, R.; Gronenborn, A. M. NMR studies on domain diffusion and alignment in modular GB1 repeats. *Biophys. J.* **2010**, *99*, 2636−2646.
(83) Sengupta, I.; Nadaud, P. S.; Helmus, J. J.; Schwieters, C. D.; Jaroniec, C. P. Protein fold determined by paramagnetic magic-angle spinning solid-state NMR spectroscopy. *Nat. Chem.* **2012**, *4*, 410−417.
(84) Nadaud, P. S.; Helmus, J. J.; Kall, S. L.; Jaroniec, C. P. Paramagnetic ions enable tuning of nuclear relaxation rates and provide long-range structural restraints in solid-state NMR of proteins. *J. Am. Chem. Soc.* **2009**, *131*, 8108−8120.
(85) Thoms, S.; Max, K. E. A.; Wunderlich, M.; Jacso, T.; Lilie, H.; Reif, B.; Heinemann, U.; Schmid, F. X. Dimer formation of a stabilized Gβ1 variant: A structural and energetic analysis. *J. Mol. Biol.* **2009**, *391*, 918−932.
(86) Morrone, A.; Giri, R.; Toofanny, R. D.; Travaglini-Allocatelli, C.; Brunori, M.; Daggett, V.; Gianni, S. GB1 is not a two-state folder: identification and characterization of an on-pathway intermediate. *Biophys. J.* **2011**, *101*, 2053−2060.
(87) Lindman, S.; Xue, W.-F.; Szczepankiewicz, O.; Bauer, M. C.; Nilsson, H.; Linse, S. Salting the charged surface: pH and salt dependence of protein G B1 stability. *Biophys. J.* **2006**, *90*, 2911−2921.
(88) Muñoz, V.; Thompson, P. A.; Hofrichter, J.; Eaton, W. A. Folding dynamics and mechanism of β-hairpin formation. *Nature* **1997**, *390*, 196−199.
(89) Bauer, M.; Xue, W.-F.; Linse, S. Protein GB1 folding and assembly from structural elements. *Int. J. Mol. Sci.* **2009**, *10*, 1552−1566.
(90) Chiang, Y.-W.; Borbat, P. P.; Freed, J. H. The determination of pair distance distributions by pulsed EPR using Tikhonov regularization. *J. Magn. Reson.* **2005**, *172*, 279−295.
(91) Brandi-Blanco, M. P.; Dumet-Fernandes, B.; González-Pérez, J. M.; Choquesillo-Lazarte, D. A redetermination of (N9-adenine-kN)-aqua[glycylglycinato(2-)-k3N,N′,O]-copper(II). *Acta Crystallogr., Sect. E: Struct. Rep. Online* **2007**, *63*, m1598.

DOI: 10.1021/acs.jpcb.8b07727
J. Phys. Chem. B 2018, 122, 10669−10677